A newly defined cullin-RING ubiquitin ligase promotes thermotolerance as part of the Intracellular Pathogen Response in *C. elegans*

Johan Panek, Kirthi C. Reddy, Robert J. Luallen, Amitkumar Fulzele, Eric J. Bennett, Emily R. Troemel*

Division of Biological Sciences, University of California, San Diego, La Jolla, CA 92093 USA

Running title: *A newly defined CRL promotes thermotolerance in C. elegans*

*Email: etroemel@ucsd.edu, Address: 9500 Gilman Dr #0349, La Jolla, CA 92093

Keywords: Proteostasis, Intracellular Infection, Intracellular Pathogen Response, *C. elegans*, heat shock, cullin, cullin-RING ubiquitin ligase complex, ubiquitylation (ubiquitination), TRIM

ABSTRACT

Intracellular pathogen infection leads to proteotoxic stress in host organisms. Previously we described a physiological program in the nematode *C. elegans* called the Intracellular Pathogen Response (IPR), which promotes resistance to proteotoxic stress and appears to be distinct from canonical proteostasis pathways. The IPR is controlled by PALS-22 and PALS-25, proteins of unknown biochemical function, which regulate expression of genes induced by natural intracellular pathogens. We previously showed that *pals-22* and *pals-25* regulate the mRNA expression of the predicted ubiquitin ligase component cullin *cul-6*, which promotes thermotolerance in *pals-22* mutants. Here we use co-immunoprecipitation studies to define protein-protein interactions in the IPR and show that PALS-22 and PALS-25 physically associate with each other. We also identify a previously uncharacterized RING domain protein in the TRIM family named RCS-1 as a core component that acts with CUL-6 to promote thermotolerance. Furthermore, we show that the Skp-related proteins SKR-3, SKR-4 and SKR-5 act redundantly to promote thermotolerance in *pals-22* mutants. These studies describe a newly defined CUL-6/RCS-1/SKR-3,4,5 cullin-RING ligase complex that promotes thermotolerance as part of the IPR in *C. elegans* and provide insight into how organisms cope with proteotoxic stress.

Maintaining protein homeostasis (proteostasis) after exposure to environmental stressors is critical for organismal survival (1). Several signaling pathways have been identified that help organisms cope with stressors that perturb proteostasis. For example, elevated temperature triggers the conserved Heat Shock Response (HSR) pathway, which helps organisms survive the toxic effects of heat (2). The HSR upregulates expression of chaperones that help with refolding of misfolded proteins, to prevent the formation of protein aggregates and restore proteostasis (1). Disruptions of proteostasis and the formation of protein aggregates in humans are associated with severe neurodegenerative and age-related diseases, such as Alzheimer's and Huntington's diseases (1, 3–5). Given the increasing incidence of such diseases and a lack of effective treatments (6, 7), new approaches are needed to identify protective mechanisms that provide resilience against proteotoxic stress.

Pathogen infection can perturb proteostasis and several studies in the nematode *Caenorhabditis elegans* have demonstrated intriguing

connections between immune responses to extracellular pathogens and canonical proteostasis pathways (8–11). More recently, examining the *C. elegans* host response to natural intracellular pathogens has uncovered a novel stress response pathway that promotes proteostasis (12, 13). Microsporidia are intracellular, fungal-like pathogens that are the most common cause of infection of *C. elegans* in the wild, with *Nematocida parisii* being the most commonly found microsporidian species in *C. elegans* (14). *N. parisii* replicates exclusively inside the *C. elegans* intestine, and the infection is associated with hallmarks of perturbed proteostasis in the host, such as the formation of large ubiquitin aggregates in the intestine (12). Interestingly, the host transcriptional response to this infection is very similar to the host transcriptional response to another natural intracellular pathogen of the *C. elegans* intestine, the Orsay virus (12, 15, 16). These molecularly distinct pathogens induce a common mRNA expression pattern in *C. elegans* that we termed the "Intracellular Pathogen Response" or IPR (13). Of note, IPR genes can also be induced by proteotoxic stress such as prolonged heat stress (distinct from short-term, high temperature 'heat shock') or proteasome blockade (12). These findings suggested that the IPR could provide protection against proteotoxic stress.

Functional insights into the IPR came from analysis of mutants that constitutively express IPR genes. Forward genetic screens identified two genes encoding proteins of unknown biochemical function called *pals-22* and *pals-25* that comprise an ON/OFF switch for the IPR, with *pals-22* acting as a repressor of *pals-25*, which is an activator of the IPR (13, 17). Upregulation of IPR gene expression in *pals-22* loss-of-function mutants is accompanied by a rewiring of *C. elegans* physiology, including increased resistance against natural pathogens like *N. parisii* and the Orsay virus, as well as slowed growth and shortened lifespan. *pals-22* mutants also have increased proteostasis capacity characterized by improved thermotolerance and lowered levels of aggregated proteins (13). All of the *pals-22* mutant phenotypes are reversed in *pals-22 pals-25* loss-of-function double mutants (17). Interestingly, these phenotypes appear to be independent of canonical proteostasis factors (13), such as the transcription factors HSF-1 and DAF-16, which mediate the HSR (18). The IPR is also independent of the proteasome bounceback response (17). This stress response is triggered by blockade of the proteasome and is mediated by the transcription factor SKN-1/Nrf, which upregulates transcription of proteasome subunits to increase degradation capacity (19–21). Instead, the IPR requires expression of a cullin gene called *cul-6*, which is transcriptionally regulated by *pals-22/pals-25* and by infection (13, 17). Cullins are components of E3 ubiquitin ligases, which are enzymes that catalyze transfer of ubiquitin onto substrate proteins in order to alter their fate (22). Based on these findings we hypothesized that CUL-6-mediated ubiquitylation of target proteins may act as a protein quality control mechanism in the IPR to respond to proteotoxic stress.

CUL-6 belongs to the cullin-RING Ligase (CRL) superfamily, which is found throughout eukaryotes and is the largest class of ubiquitin ligases (23). CRLs are multi-subunit enzyme complexes, a subset of which are Skp, cullin, F-box (SCF) complexes consisting of four subunits: a RING-box/RBX protein, a Skp, a cullin and an F-box protein. Due to the large number of SCF genes and their modular nature, there are many different enzyme combinations and thus a large number of different substrates that can be targeted by these enzymes. Interestingly, the SCF class of ubiquitin ligases appears to have undergone a significant expansion in the evolutionary lineage that gave rise to the nematode *C. elegans* (24, 25). For example, in comparison to other metazoans, *C. elegans* has a much larger number of F-box proteins, which serve as substrate adaptors and confer specificity to SCF ligases. There are around 520 F-box proteins in the *C. elegans* genome (24), in comparison to around 68 in humans (26), 22 in *Drosophila* and 11 in *Saccharomyces cerevisiae* (27). In addition, the number of core SCF components has increased in nematodes, with *C. elegans* having 22 Skp-related proteins in comparison to six in *Drosophila*, just one in *S. cerevisiae*, and one in

humans (28). The SCF components upregulated as part of the IPR include not only *cul-6* as mentioned above, but also the Skp-related proteins *skr-3, skr-4 and skr-5* (12). If *cul-6* were functioning as part of a ubiquitin ligase complex to promote proteostasis as part of the IPR, it should be acting with *skrs* and other CRL components.

Here we describe how CUL-6 promotes proteostasis as part of a novel CRL complex in *C. elegans*. First, we show that tissue-specific expression of *cul-6* in either the intestine or in the pharynx can promote thermotolerance. Importantly, we found that CUL-6 requires a conserved neddylation site to promote thermotolerance, indicating that its activity is regulated via a canonical NEDD8 modification, which is a hallmark of bona fide CRLs (29). To identify other components in this complex we performed co-immunoprecipitation with CUL-6, as well as with PALS-22 and PALS-25, which are antagonistic paralogs that regulate expression of IPR genes (17). We found that PALS-22 and PALS-25 proteins physically associate, indicating that they interact not only genetically, but also biochemically. We also identified several CUL-6 interaction partners, including a previously uncharacterized RING domain protein called C28G1.5. We generated deletion mutations of C28G1.5 and found that they suppressed the increased thermotolerance of *pals-22* mutants, just like *cul-6* mutations. Testing different combinations of *skr-3, skr-4* and *skr-5* double mutants we found these *skr* genes act redundantly to promote thermotolerance in *pals-22* mutants. Finally, we developed an RNAi system to test the role of other proteins that promote thermotolerance in a *pals-22* mutant background. In summary, this work demonstrates that CUL-6 is part of a newly defined CRL that promotes thermotolerance as part of the IPR, and broadens our understanding of how animals survive exposure to proteotoxic stress such as heat shock.

Results

The cullin CUL-6 acts in the intestine and pharynx to promote thermotolerance

In comparison to wild type animals, *pals-22* loss-of-function mutants have increased thermotolerance, which is reduced to wild-type levels in *pals-22; cul-6* double mutants. Our previous results indicated that *pals-22* regulates thermotolerance in the intestine, where it also regulates *cul-6* mRNA expression (13). Because *cul-6* is expressed in the both the intestine and the pharynx, we sought to determine in which of these tissues *cul-6* acts to promote thermotolerance. Therefore, we designed tissue-specific rescue constructs with *cul-6* cDNA using the Mos1-mediated Single Copy Insertion (MosSCI) system (30). With the MosSCI technique, we drove expression of GFP-tagged versions of *cul-6* using intestinal (*vha-6p*) or pharyngeal promoters (*myo-2p*). We found that both the intestinal and pharyngeal rescue strains expressed GFP::CUL-6 with the expected tissue distribution pattern (Figure 1A). We then crossed these tissue-specific CUL-6 MosSCI transgenes into *pals-22; cul-6* double mutants to test for rescue of thermotolerance. Here we found that expression of *cul-6* in either the intestine or the pharynx was sufficient to increase the thermotolerance of *pals-22; cul-6* double mutants (Figure 1B).

Our previous results demonstrated that *cul-6* had a role in proteostasis only in a *pals-22* mutant background, and not in a wild-type background (13). This finding suggested that *cul-6* affects proteostasis only when it is overexpressed compared to wild-type animals, such as in *pals-22* mutants. Consistent with this model, here we found that overexpression of CUL-6 from a multi-copy array (CUL-6 tagged at the C-terminus with GFP and 3xFLAG, surrounded by ~20kb endogenous regulatory region (31)) led to increased thermotolerance compared to wild-type animals (Fig. 1B). Furthermore, we found that either pharyngeal or intestinal expression of *cul-6* cDNA in a wild type background promoted thermotolerance (Figure 1B). Importantly, transgenic strains with *vha-6* and *myo-2* promoters driving genes other than wild-type *cul-6* did not have increased thermotolerance (see text below, and Figure 1B). Thus, increased expression of *cul-6* in a wild-type background in either the intestine or the pharynx leads to increased thermotolerance.

We were curious if expressing *cul-6* in tissues where it is not normally expressed would also promote thermotolerance. Therefore, we generated a *myo-3p::cul-6* construct to determine whether expression in body wall muscle could promote thermotolerance. Surprisingly, we found that *cul-6* expression in body wall muscle appeared to be toxic, because we failed to recover *myo-3p::cul-6* transgenic animals after several rounds of germline injections. To perform a careful assessment of lethality, we injected either red fluorescent protein markers together *myo-3p::cul-6*, or red fluorescent protein markers alone (see Materials and Methods). Here we found none of the eggs expressing red fluorescent protein markers hatched when co-injected with *myo-3p::cul-6* (0/87), while more than half of the eggs hatched when injected with the red fluorescent protein markers alone (48/84). The reason for toxicity of *cul-6* expression in body wall muscle is unclear.

The activity of cullin-RING ubiquitin ligases can be regulated by neddylation, which is the process of conjugating the ubiquitin-like protein Nedd8 onto a cullin protein at a conserved lysine residue (29). To determine whether CUL-6 might be regulated by neddylation, we identified the lysine residue that would likely be targeted for neddylation and mutated this residue into an arginine, which would be predicted to disrupt neddylation (Supplementary Figure 1) (32). We used the MosSCI technique to generate a strain that contains this *vha-6p::cul-6(K673R)* transgene (expression visualized in Figure 1A), and found that it could not rescue the thermotolerance of *pals-22*; *cul-6* mutants (Figure 1B). Furthermore, unlike *vha-6p::cul-6(wild-type)*, the *vha-6p::cul-6(K673R)* transgene did not promote thermotolerance in a wild-type background. These results suggest that CUL-6 requires neddylation to promote thermotolerance, which is consistent with CUL-6 acting as part of a ubiquitin ligase complex.

Co-immunoprecipitation/mass spectrometry analysis identifies CUL-6 binding partners

To identify the components of a CUL-6-containing ubiquitin ligase complex, we performed co-immunoprecipitation mass spectrometry (co-IP/MS) analysis to identify binding partners of CUL-6. Here we used the *C. elegans* strain with GFP::3xFLAG-tagged CUL-6, which is functional for thermotolerance (Figure 1). We also used similar GFP::3xFLAG-tagged strains for PALS-22 and PALS-25 (13, 17), which regulate mRNA expression of *cul-6* and other IPR genes. Through analysis of binding partners for PALS-22 and PALS-25, we sought to obtain insight into their biochemical function, which is currently unknown. Two proteins, GFP::3xFLAG alone and an unrelated protein F42A10.5::GFP::3xFLAG, were added as controls for the co-IPs.

We confirmed transgene expression using immunoblotting and microscopy analysis. First, western analysis indicated that all five fusion proteins showed bands of the predicted molecular weight (Supplementary Figure 2A). Second, when we treated animals with the proteasome inhibitor Bortezomib to induce proteotoxic stress and IPR gene expression, we saw an increase in CUL-6 expression by both western and microscopy analysis, as expected from previous studies (Supplementary Figure 2A-B). As mentioned above, expression of CUL-6 is seen most strongly in the pharynx and the first two rings of the intestine. PALS-22 and PALS-25 are broadly expressed throughout animal and their expression is not affected by IPR activation (17).

We then performed three independent co-IP/MS experiments with these FLAG-tagged transgenic strains. Animals were treated with Bortezomib to induce IPR gene expression, proteins were extracted, and then subjected to IP with anti-FLAG antibodies. Mass spectrometry analysis was performed on the IP material and spectral counts were used to calculate the fold change and adjusted p-values between the experimental IPs and the control IPs (Supplementary Table 1). Proteins that were significantly more abundant in the experimental IP compared to either of the control IP's (GFP alone control or F42A10.5 control, at adjusted p-value < 0.05 and log2 fold change > 1), were considered interacting proteins (Supplementary Table 1).

Co-IP/MS of PALS-22 identified 23 binding partners, including PALS-25 as one of the most

highly enriched binding partners, as compared to co-IP/MS of control proteins (Supplementary Figure 3). PALS-22 also is physically associated with PALS-23, which is a PALS protein of unknown function, as well as with F26F2.1, which is a protein of unknown function induced by the IPR (12). Co-IP/MS of PALS-25 identified 7 binding partners, with PALS-22 being by far the most highly enriched hit when compared with co-IP/MS of either control protein. These reciprocal co-IP results indicate that PALS-22 and PALS-25 physically associate with each other, perhaps directly binding to each other.

Co-IP/MS of CUL-6 identified 26 significant binding partners. These proteins included predicted SCF ubiquitin ligase components, such as the Skp-related protein SKR-3 and the F-box proteins FBXA-75 and FBXA-158 (Figure 2A, B). Additionally, 6 subunits of the 26S proteasome were identified (RPT-3, 4 and RPN-5, 6.1, 8, 9). An SCF ubiquitin ligase complex canonically contains an RBX RING box protein, which interacts both with a cullin and with an E2 enzyme to stimulate ubiquitin chain formation on targets recognized by an F-box protein in the complex. *C. elegans* has two RBX proteins, RBX-1 and RBX-2, but neither of these proteins were identified as significant binding partners for CUL-6 in the co-IP/MS. Therefore, we searched for other CUL-6 binding proteins that have a RING domain. Here, we identified a single candidate, C28G1.5. Because of results described below, we renamed C28G1.5 as RING protein acting with cullin and Skr proteins (RCS-1). Interestingly, *rcs-1* mRNA expression, like *cul-6* mRNA expression, is higher in *pals-22* mutants compared to wild-type animals (log2 FC=2.81, adjusted p-value= 4.83E-08), and in *pals-22* mutants compared to *pals-22 pals-25* mutants (log2 FC=2.10, adjusted p-value=3.898E-07) (17).

RING domain protein RCS-1 acts with CUL-6 to promote thermotolerance in pals-22 mutants

The *rcs-1* gene had no previously described role in *C. elegans*, and has two isoforms: *rcs-1b* has a RING domain and a B-box domain, and *rcs-1a* has the RING domain only (Figure 3A). The closest potential ortholog of *rcs-1* in humans is the tripartite motif-containing protein 23 (TRIM23). The TRIM family is named for having three motifs (RING finger, B box domain, and coiled coil domain), and many TRIM proteins have E3 ubiquitin ligase activity (33). However, RCS-1 and TRIM23 do not appear to be orthologous, as sequence comparison of TRIM23 against the *C. elegans* genome identifies other *C. elegans* RING proteins as closer matches than RCS-1 (see below). To investigate how RCS-1 is related to TRIM23, and other *C. elegans* RING and TRIM proteins, we performed phylogenetic analysis of the full-length RCS-1 (RCS-1B) using a Bayesian inference method (Supplementary Figure 4). Based on this analysis, RCS-1 seems to be part of the *C. elegans* TRIM protein family (34). However, several *C. elegans* proteins like the ADP-Ribosylation Factor related proteins (ARF-3 and ARF-6) are more closely related to TRIM23 than RCS-1 is. In addition, RCS-1 does not seem to be closely related to *C. elegans* RING proteins RBX-1 or RBX-2.

To investigate the role of RCS-1 in promoting thermotolerance with CUL-6, we used a CRISPR-Cas9 strategy to generate deletion alleles of *rcs-1*. Two full deletion alleles of *rcs-1* (*jy84* and *jy105*) were generated, and then crossed in *pals-22* mutants. Here we found for both *rcs-1* alleles that *pals-22; rcs-1* double mutants had thermotolerance similar to wild-type animals, indicating that *rcs-1* is required for the increased thermotolerance of *pals-22* mutants (Figure 3B, C). If RCS-1 were acting in a CRL together with CUL-6, then loss of *rcs-1* would not further lower thermotolerance in a *pals-22; cul-6* mutants. Indeed, we found that *pals-22; cul-6; rcs-1* triple mutants had a similar level of thermotolerance to *pals-22; cul-6* mutants, as well as to *pals-22; rcs-1* mutants and wild-type animals. These findings, together with CUL-6 co-IP results, are consistent with RCS-1 being the RING domain protein that acts with CUL-6 in a ubiquitin ligase complex.

SKP-related proteins SKR-3, SKR-4 and SKR-5 act redundantly to promote thermotolerance in pals-22 mutants

In addition to a cullin and a RING protein, SCF ubiquitin ligase complexes contain a Skp protein.

Expression of three Skp-related proteins (*skr-3, skr-4 and skr-5*) is upregulated by both intracellular infection and mutation of *pals-22*, similar to *cul-6* expression (12, 13). Thus, we speculated that these genes might act together with *cul-6* in an SCF complex. However, we previously found that mutation of either *skr-3, skr-4* or *skr-5* alone in a *pals-22* mutant background had no effect on thermotolerance (13). Therefore, we examined whether there may be redundancy among these genes. We made all of the possible combinations of *skr-3, skr-4* and *skr-5* as double mutants and then crossed them into a *pals-22* mutant background. Here we found that *pals-22; skr-3 skr-5* and *pals-22; skr-5 skr-4* triple mutants had a significant reduction in thermotolerance compared to *pals-22* mutants, with levels similar to wild type animals. In contrast, *pals-22; skr-3 skr-4* mutants had thermotolerance similar to *pals-22* mutants (Figure 4B). These results indicate that either SKR-3, SKR-4, or SKR-5 individually can act together with CUL-6 in a SCF to promote thermotolerance. However, SKR-3 and SKR-4 only seem to be important if SKR-5 has been lost, whereas SKR-5 is important if either SKR-3 or SKR-4 has been lost. Interestingly, *skr-3* and *skr-4* share high sequence homology, and *skr-5* is the most highly induced *skr* gene in *pals-22* mutants, suggesting that *skr-5* may play a unique role (13). Importantly, none of the double mutants had an effect on thermotolerance in a wild-type background, consistent with their acting in a complex with *cul-6*, which also does not affect thermotolerance when mutated in a wild-type background.

In addition to regulating thermotolerance, *pals-22* also regulates developmental rate of *C. elegans*, with *pals-22* mutants being slower to develop to the fourth larval (L4) stage compared to wild-type animals. Our previous analysis indicated that while *cul-6* mutations suppress the effect of *pals-22* on thermotolerance, they do not suppress the effects of *pals-22* on developmental rate. Similarly, we found that mutations in *rcs-1*, *skr-3 skr-4*, *skr-3 skr-5*,or *skr-5 skr-4* do not suppress the slowed developmental rate in *pals-22* mutants (Supplementary Figure 5).

To confirm the phenotypes observed using the *skr* mutant allele and to more easily analyze factors that may be functionally redundant, we sought to use RNA interference (RNAi) in lieu of generating mutants and performing crosses. However, we found that *pals-22* mutants do not have increased thermotolerance compared to wild type animals when fed on the standard *E. coli* bacteria used for feeding RNAi (HT115) (Supplementary Figure 6A). This effect is likely due to dietary differences between HT115 and the OP50 strain used for thermotolerance experiments described above (35). Therefore, we tested thermotolerance on the OP50 strain (R)OP50 that was modified to enable feeding RNAi studies (36). Here we found that *pals-22* mutant animals fed on these RNAi-competent OP50 bacteria (transformed with empty vector L4440) have increased thermotolerance compared to wild type animals, which is restored back to wild type levels in *pals-22; cul-6* mutants (Supplementary Figure 6A). This system thus enables RNAi analysis of factors that promote thermotolerance in a *pals-22* mutant background. Using this system, we were able to successfully transfer the *cul-6* RNAi clone into this strain, and we confirmed that RNAi knocked down expression of *cul-6*, by measuring reduction of expression from a CUL-6::GFP::3xFLAG transgene (Supplementary Figure 6B, C). We also found that *cul-6* RNAi suppressed the enhanced thermotolerance of *pals-22* mutants (Supplementary Figure 6D). With this system, we confirmed that *skr-3* and *skr-5* act redundantly to promote thermotolerance, as RNAi against *skr-3* in a *skr-5* mutant background suppressed thermotolerance of *pals-22* mutants (Figure 4C). Thus, this improved RNAi system provides an independent means of assessing the role of factors that regulate thermotolerance in a *pals-22* mutant background. Altogether, these studies indicate that a RCS-1/CUL-6/SKR-3,4,5 ubiquitin ligase complex promotes thermotolerance in *C. elegans*.

Discussion

Thermal stress is one of many types of proteotoxic stress that can impair organismal health and survival. Here we used a combination of genetics and biochemistry to broaden our

understanding of a recently identified proteostasis pathway called the IPR, which enables animals to survive exposure to thermal stress in a manner distinct from the canonical heat shock response (HSR). Specifically, we demonstrate that the IPR involves the CUL-6/cullin acting as part of newly described ubiquitin ligase that appears to function in either the intestine or the pharynx of *C. elegans*. This CUL-6-containing CRL includes a previously uncharacterized RING protein we named RCS-1, as well as the Skp-related proteins SKR-3, SKR-4, and SKR-5 (Figure 5). We propose that this RCS-1/CUL-6/SKR-3,4,5 ubiquitin ligase complex is able to target proteins for ubiquitin-mediated proteasomal degradation and that this activity is a critical part of the IPR program. Consistent with this model, our co-IP/MS identified several proteasomal subunits that interact with CUL-6.

We also investigated protein-protein interactions of the PALS-22 and PALS-25 proteins, which comprise an ON/OFF switch in the IPR that regulates mRNA expression of *cul-6, skr-3,4,5* and *rcs-1*. Previous studies indicated that *pals-22* and *pals-25* are in the same operon and interact genetically, and our co-IP/MS studies indicate they also interact biochemically. Notably, the *pals* gene family has expanded in the *C. elegans* genome, with 39 genes in *C. elegans*, in comparison to only 1 *pals* gene each in mouse and human (37). The only PALS proteins with identified phenotypes are PALS-22 and PALS-25, and it will be interesting to determine the phenotypes of the other *pals* genes in *C. elegans*, as well as the role of the single *pals* homolog in mammals. Although the divergent '*pals'* protein signature that defines PALS proteins is of unknown function, PALS-22 does have weak homology with F-box proteins (37), leading to the speculative idea that PALS proteins function as adaptor proteins in ubiquitin ligase complexes. Biochemical studies of PALS-22 and PALS-25 will help elucidate how these antagonistic paralogs control expression of IPR genes, including SCF ligase components like *cul-6*, *skr-3,4,5* and *rcs-1*.

C. elegans has a greatly expanded repertoire of SCF ligase components. This expansion has been suggested to reflect the results of an arms race against intracellular pathogens, as SCF components are among the most rapidly diversifying genes in the *C. elegans* genome (25). The most dramatically expanded class of SCF components includes ~520 F-box adaptor proteins in *C. elegans* (24). *C. elegans* also has 22 SKR proteins, in comparison to only 1 Skp in humans, indicating there has been an expansion of core SCF components as well. Here we identified SKR-3 as a binding partner for CUL-6, which is consistent with previous 2-hybrid results (28). Interestingly, we found redundancy in the role of SKRs at the phenotypical level: either SKR-3, SKR-4 or SKR-5 appear capable of acting with CUL-6 to promote thermotolerance.

Canonical CRLs contain an RBX protein as the RING domain protein (23). *C. elegans* has only two RBX proteins, RBX-1 and RBX-2, suggesting that there was not expansion of these core components in *C. elegans*. However, our co-IP/MS studies with CUL-6 did not identify these proteins as interacting partners for CUL-6, but rather identified RCS-1. Given our genetic and biochemical results, we propose that RCS-1 plays the same role as an RBX protein would in a canonical SCF complex (Figure 5). RCS-1 does not have a clear human ortholog, but the closest human protein is TRIM23 (38). Interestingly, the TRIM family contains 68 genes in humans, many of which encode single subunit E3 ubiquitin ligases, including those that restrict viral infection, and regulate inflammatory signaling (33). *C. elegans* has 18 TRIM proteins, and they appear to have a simpler structure than human TRIM proteins, in that they do not have additional motifs in the C-terminal domains, which are found in the majority of mammalian TRIM proteins (34). If these other *C. elegans* TRIM proteins can act in SCF ligases like RCS-1, it indicates there may also be an expansion of the RING core SCF components in *C. elegans*, in addition to the previously described expansion of SKRs and adaptor proteins.

The role of CUL-6 in promoting thermotolerance was first demonstrated in *pals-22* mutants, where there is overexpression of

CUL-6, as well as several other SCF components, including *skr-3,4,5* and *rcs-1* (13, 17). However, here we found that animals overexpressing only CUL-6, without the other components of the SCF, have increased thermotolerance. One explanation for this result is that CUL-6 is the limiting factor in a SCF that promotes thermotolerance in the IPR. Consistent with this idea, other components of the complex like SKR-3,4,5 are functionally redundant for thermotolerance, so even basal expression level might be sufficient to build a functional SCF, once CUL-6 expression increases past a certain threshold level. Of note, we have yet to find a phenotype for *cul-6* mutants in a wild-type background using a standard heat shock resistance assay. This assay uses an acute heat shock, a stressor that is not sufficient to upregulate *cul-6* expression: previous studies showed that prolonged heat stress is required to induce *cul-6* and other IPR gene expression (12, 13, 39). Perhaps through a combination of prolonged heat stress to induce *cul-6* expression, followed by acute heat shock to induce lethality, we may find a role for *cul-6* mutants in a wild-type background. If so, upregulation of a RCS-1/CUL-6/SKR-3,4,5 ubiquitin ligase complex might be part of a chronic heat stress response that follows the acute response, mediated by the canonical HSR.

What substrate adaptor protein(s) acts in the RCS-1/CUL-6/SKR-3,4,5 ubiquitin ligase complex, and what substrate(s) does it target? It is possible that the effects of this complex are mediated through targeting a single regulatory protein for ubiquitylation and degradation. For example, ubiquitylation of the DAF-2 insulin receptor by the ubiquitin ligase CHIP can alter DAF-2 trafficking, and it appears that ubiquitylation of just this one target has significant effects on proteostasis in *C. elegans* (40). In contrast, CRL2 and CRL4 complexes in humans have recently been shown to target the C-termini of a large number of proteins for degradation as part of a newly identified protein quality control system (41, 42), Given the modular nature of the SCF ligase family, the large number of F-box substrate adaptor proteins in *C. elegans*, and the redundancy we found in the SKR-3,4,5 proteins, it seems possible that there are multiple substrates and adaptors used in the IPR. An exciting possibility is that the IPR involves distinct CRLs that ubiquitylate several different targets to improve proteostasis and tolerance against environmental stressors, including infections. Identifying these factors will be the subject of future studies.

Experimental Procedures

Cloning and generation of cul-6 tissue-specific rescue strains

A full list of constructs and strains used in this study is in Supplementary Table 2. To generate the *vha-6p::CUL-6* transgene (pET499), *vha-6p::SBP::3XFLAG*, *cul-6* cDNA, and the *unc-54* 3' UTR were assembled in pCFJ150 using Gateway LR. To generate *myo-2p::CUL-6* (pET686) and *myo-3p::CUL-6* (pET687) constructs, the promoters *myo-2p*, *myo-3p* and the pET499 linearized backbone without *vha-6p* promoter were amplified by PCR from pCFJ90, pCFJ104 and pET499, respectively and assembled by Gibson recombination (43). To generate the *cul-6(K673R)* construct (pET688), a 86 bp single strand oligonucleotide and a linearized pET499 backbone that had been amplified by PCR were assembled by Gibson recombination. To generate the *vha-6p::3XFLAG::GFP* (pET554) transgene, *vha-6p::3XFLAG::GFP* and *let-858* 3' UTR were assembled in pCFJ150 using Gateway LR. Mos1-mediated Single Copy Insertion (MosSCI) was performed as described previously (30). Briefly, the plasmid of interest (25 ng/µl) was injected with pCFJ601 (50 ng/µl), pMA122 (10 ng/µl), pGH8 (10 ng/µl), pCFJ90 (2.5 ng/µl), and pCFJ104 (5 ng/µl) into the EG6699 strain. Injected animals were incubated at 25°C for 7 days and then subjected to heat shock for 2h at 34°C. After 5 h non-Unc animals were selected and the presence of the insertion was verified by PCR and sequencing.

Transgenic strains with TransgeneOme fosmids (Supplementary Table 2) were generated as extrachromosomal arrays (31) by injecting into *ttTi5605; unc-119(ed3)* worms (strain EG6699) and then selecting non-Unc worms.

Lethality scoring of myo-3p::cul-6 tissue-specific rescue strains

To score the lethality of *myo-3p::cul-6* expression, worms were injected with a complete MosSCI mix (see above) containing either *myo-3p::cul-6* as the plasmid of interest, or water. Injected animals were incubated at 25°C and after 1 day, eggs expressing red fluorescence were transferred onto new plate at 25°C for 24 h. The hatching ratio of transferred eggs was then scored for both conditions. The assay was repeated two independent times.

Thermotolerance assays

Animals were grown on standard NGM plates at 20°C. L4 stage animals were transferred onto fresh NGM plates seeded with OP50-1 and then subjected to heat shock for 2 h at 37.5°C. The plates were then placed in a single layer on a benchtop at room temperature for 30 min, and then transferred to a 20°C incubator. Then, 24 h later the survival was scored in a blinded manner. Worms not responding to touch were scored as dead, and 30 worms were scored per plate. Three replicate plates were scored for each strain per experiment, and each experiment was performed at least three independent times. Statistical significance was tested using one-way ANOVA and Tukey's HSD for post-hoc multiple comparisons.

Co-immunoprecipitation

Each sample for co-IP/MS was prepared in 3 independent experimental replicates. For each sample, 200,000 synchronized L1 animals were transferred onto NGM plates and grown for 48 h at 20°C. Bortezomib was added to reach a final concentration of 22 µM or the equivalent volume of DMSO for the control plates. After 6 h at 20°C worms were washed off of the plates with M9, washed twice with M9, resuspended in 500 µl of ice-cold lysis buffer (50mM HEPES, pH7.4, 1mM EGTA, 1mM MgCl2, 100mM KCl, 1% glycerol, 0.05% NP40, 0.5mM DTT, 1x protease inhibitor tablet) and immediately frozen dropwise in liquid N_2. Frozen pellets were ground into powder with a pre-chilled mortar and pestle. Protein extracts were spun for 15 min 21,000g at 4°C and supernatants were filtered on 0.45 µm filters (WHATMAN). Protein concentration was determined using Pierce 660nm protein assay and adjusted to 1 µg/µl with fresh lysis buffer. 1 mg of each sample was mixed with 25 µl of ANTI-FLAG M2 Affinity Gel (Sigma) and incubated at 4°C with rotation (12 rpm) for 1h. The resin was washed twice with 1 ml lysis buffer, twice with 1 ml lysis buffer for 5min, twice with 1 ml wash buffer (50mM HEPES, pH7.4, 1mM MgCl2, 100mM KCl) and 20min with 1 ml wash buffer with rotation. The liquid was removed and the beads were then stored at -80°C.

Trypsin digestion

The immunoprecipitated proteins bound to the beads were digested overnight in 400 ng trypsin (Sigma, V511A) in 25 mM ammonium bicarbonate (Sigma) at 37°C. Samples were then reduced with 1mM final concentration of Dithiothreitol (DTT, Acros Organics) for 30min and alkylated with 5mM final concentration of Iodoacetamide (IAA, MP Biomedicals, LLC) for 30min in dark. The peptides were extracted from the beads by adding 50 µL of 5% Formic acid (Sigma). The extraction was repeated one more time and the eluted peptides were combined. Digested peptides were desalted using Stage-Tip, C18 peptide cleanup method. The eluates were vacuum dried, and peptides were reconstituted in 15 µL of 5% Formic acid, 5% Acetonitrile solution for LC-MS-MS analysis.

LC-MS-MS Analysis

Samples were analyzed in triplicate by LC-MS-MS using an EASY-nLC 1000 HPLC (Thermo Scientific) and Q-Exactive mass spectrometer (Thermo Scientific, San Jose, CA) as described previously (44) with the following modifications. The peptides were eluted using a 60min acetonitrile gradient (45 min 2%-30% ACN gradient, followed by 5 min 30-60% ACN gradient, a 2min 60-95% ACN gradient, and a final 8min isocratic column equilibration step at 0% ACN) at 250nL/minute flow rate. All the gradient mobile phases contained 0.1% formic acid. The data dependent analysis (DDA) was done using top 10 method with a positive polarity, scan range 400-1800 m/z, 70,000 resolution, and an AGC target of 3e6. A dynamic exclusion time of 20 s was implemented and unassigned, singly charged and charge states above 6 were excluded for the data dependent MS/MS scans. The MS2 scans were triggered with a minimum AGC target

threshold of 1e5 and with maximum injection time of 60 ms. The peptides were fragmented using the normalized collision energy (NCE) setting of 25. Apex trigger and peptide match settings were disabled.

Peptide and Protein Identification and Quantification

The RAW files obtained from the MS instrument were converted into mzXML format. The SEQUEST search algorithm was used to search MS/MS spectra against the concatenated target decoy database comprised of forward and reverse, reviewed *C. elegans* FASTA sequences from Uniprot (downloaded on 6/8/2015) along with GFP and *E. coli* sequences appended in the same file. The search parameters used were as follows: 20 ppm peptide mass tolerance; 0.01 Da fragment ion tolerance; Trypsin (1 1 KR P) was set as the enzyme; maximum 2 missed cleavages were allowed; Oxidation on methionine (15.99491 Da) and n-term acetylation (42.01056 Da) were set as differential modifications; static modification (57.02146 Da) was set on cysteine for alkyl modification. Peptide matches were filtered to a peptide false discovery rate (FDR) of 2% using the linear discrimination analysis. The protein level matches were filtered at 2% FDR using the protein sieve analysis. The spectral counts from the triplicates were then summed and used for the data analysis.

Analysis of mass spectrometry data

Peptide spectral counts were used to calculate fold change ratio, p-value and adjusted p-value between sample IPs and control IPs (GFP and F42A10.5) using the DEP package in R (45). Briefly the data were filtered to keep only the peptides present in at least two replicates in one condition. Filtered data were normalized using Variance Stabilizing Normalization. Missing values were imputed using the MiniProb method from the DEP package by randomly selecting values from a Gaussian distribution centered on a minimal value of the dataset. Fold change ratio and adjusted p-values were calculated. Proteins were considered as significant with adjusted p-value < 0.05 and log2 fold change > 1. Any protein with a negative log2 fold change with one control or the other (*i.e.* more affinity to the control protein than the tested bait) was considered as non-significant.

Phylogenic analysis of RCS-1

Amino acid sequences of 15 proteins were aligned using MUSCLE (version 3.7) and trimmed with trimAI (version 1.3) (46) using phylemon2 online platform (47). Bayesian Markov chain Monte Carlo inference (LG + I + G + F) was performed using BEAST (version 1.10.4) (48). Analysis was run using a Yule model tree prior, an uncorrelated relaxed clock (lognormal distribution) and a chain length of 10 million states sampled every 1,000 iterations. Results were assessed with Tracer (version 1.7.1), maximum clade credibility tree was built after a 25% burn-in. Posterior probability values greater than 0.5 are marked on branch labels.

CRISPR deletion of rcs-1

To generate the 2.18 kb deletion alleles of *rcs-1*, a co-CRISPR strategy was used, adapted from the IDT proposed method for *C. elegans*. We designed two crRNA encompassing the whole *rcs-1* locus (crRNA1: 5'-GTTTGTTGAAGGAAATGCACAGG-3', crRNA2: 5'-GGTTTCCTATAGCTGTGACACGG-3'). These two oligonucleotides were synthetized by IDT, and used with a crRNA targeting the *dpy-10* gene (*dpy-10* crRNA3:5'-GCTACCATAGGCACCACGAG-3') and assembled with commercial tracrRNA (50 µM crRNA1 and crRNA2, 25 µM *dpy-10* crRNA, and 40 µM tracrRNA). After an annealing step for 5 min at 95°C, the resulting guide RNA mixture was added to CAS9-NLS protein (27 µM final – ordered from QB3 Berkeley) and microinjected into N2 worms. F1 Dpy progeny were screened by PCR for a deletion and positive lines were backcrossed 4 times to the N2 background before testing.

RNA interference assays

RNA interference assays were performed using the feeding method. Overnight cultures of HT115 or OP50 strain (R)OP50 modified to enable RNAi (36) (gift from Meng Wang lab, Baylor College of Medicine) were plated on RNAi plates (NGM plates supplemented with 5 mM IPTG, 1 mM carbenicillin) and incubated at

20°C for 3 days. Gravid adults were transferred to these plates, and their F1 progeny (L4 stage) were transferred onto new RNAi plates before being tested for thermotolerance as previously described.

Western blot analysis

For each strain, 1500 synchronized L1 worms were placed on NGM plates seeded with OP50 bacteria and incubated at 20°C for 48 h. These animals were then treated with Bortezomib (22 µM final) or control DMSO for 6 h and washed off the plate with M9. Proteins were extracted in 200µl lysis buffer (50 mM HEPES, pH7.4, 1 mM EGTA, 1 mM MgCl2, 100 mM KCl, 1% glycerol, 0.05% NP40, 0.5 mM DTT, 1x protease inhibitor tablet) as previously described (13). Protein levels were determined using the Pierce 660nm assay. Equal amount of proteins (5 µg) were boiled in protein loading buffer, separated on a 5-20% SDS-PAGE precast gel (Bio-Rad) and transferred onto PVDF membrane. Nonspecific binding was blocked using 5% nonfat dry milk in PBS-Tween (0.2%) for 1 hour at room temperature. The membranes were incubated with primary antibodies overnight at 4°C (mouse anti-FLAG diluted 1:1,000 and mouse anti-Tubulin diluted 1:7,500), washed 5 times in PBS-Tween and blotted in horseradish peroxidase-conjugated secondary antibodies at room temperature for 2 h (Goat anti-mouse diluted 1:10,000). Membranes were then washed 5 times in PBS-Tween, treated with ECL reagent (Amersham), and imaged using a Chemidoc XRS+ with Image Lab software (Bio-Rad).

Florescence microscopy

For *cul-6* tissue-specific expression lines shown in Figure 1, images were taken using a Zeiss LSM700 confocal microscope with 10X and 40X objectives. For RNAi knock-down in Supplementary Figure 6, L4 stage F1 progeny of ERT422 worms fed with OP50 expressing *cul-6* RNAi were anesthetized using 10 µM levamisole in M9 buffer and mounted on 2% agarose pads for imaging with a Zeiss LSM700 confocal. Using ImageJ software (version 1.52e), GFP signal in the pharynx and the first intestinal cells ring was measured, as well as three adjacent background regions. The total corrected fluorescence (TCF) was calculated as TCF = integrated density – (area of selected cell × mean fluorescence of background readings). For each condition, 30 worms were imaged. Significance was assay with Student's t-test.

Measurement of developmental rate

40 – 50 gravid adults were transferred onto standard 10 cm NGM plate and incubated at 20°C to lay eggs for 2h before being removed. These plates were incubated at 20°C and the proportion of eggs that hatched and developed into L4's was scored at 48 h, 64 h, and 72 h by scoring 100 animals each replicate.

Acknowledgements: We thank Spencer Gang, Vladimir Lazetic, Ivana Sfarcic, Jessica Sowa, and Eillen Tecle for comments on the manuscript. This work was supported by NIH under R01 AG052622 to ERT and EJB, and a Burroughs Wellcome Fund Investigators in the Pathogenesis of Infectious Diseases fellowship to ERT.

Conflict of interest: The authors declare that they have no conflicts of interest with the contents of this Article.

The content is solely the responsibility of the authors and does not necessarily represent the official views of the National Institutes of Health.

Author contributions: JP, ERT and EJB designed the experiments. JP, KCR, AF, RJL and ERT performed the experiments and analyzed the results. JP wrote the paper with ERT.

References

1. Labbadia, J., and Morimoto, R. I. (2015) The biology of proteostasis in aging and disease. *Annu. Rev. Biochem.* **84**, 435–64
2. Gomez-Pastor, R., Burchfiel, E. T., and Thiele, D. J. (2017) Regulation of heat shock transcription factors and their roles in physiology and disease. *Nat. Rev. Mol. Cell Biol.* **19**, 4–19
3. Hipp, M. S., Park, S.-H. H., and Hartl, F. U. (2014) Proteostasis impairment in protein-misfolding and -aggregation diseases. *Trends Cell Biol.* **24**, 1–9
4. Taylor, R. C., and Dillin, A. (2011) Aging as an Event of Proteostasis Collapse. *Cold Spring Harb. Perspect. Biol.* **3**, a004440–a004440
5. Kourtis, N., and Tavernarakis, N. (2011) Cellular stress response pathways and ageing: intricate molecular relationships. *EMBO J.* **30**, 2520–2531
6. Roberson, E. D., and Mucke, L. (2006) 100 years and counting: prospects for defeating Alzheimer's disease. *Science*. **314**, 781–4
7. Alzheimer's Association (2015) 2015 Alzheimer's disease facts and figures. *Alzheimers. Dement.* **11**, 332–84
8. Mohri-Shiomi, A., and Garsin, D. A. (2008) Insulin signaling and the heat shock response modulate protein homeostasis in the Caenorhabditis elegans intestine during infection. *J. Biol. Chem.* **283**, 194–201
9. Tillman, E. J., Richardson, C. E., Cattie, D. J., Reddy, K. C., Lehrbach, N. J., Droste, R., Ruvkun, G., and Kim, D. H. (2018) Endoplasmic Reticulum Homeostasis Is Modulated by the Forkhead Transcription Factor FKH-9 During Infection of *Caenorhabditis elegans*. *Genetics*. **210**, 1329–1337
10. Singh, V., and Aballay, A. (2006) Heat-shock transcription factor (HSF)-1 pathway required for Caenorhabditis elegans immunity. 10.1073/pnas.0604050103
11. Pellegrino, M. W., Nargund, A. M., Kirienko, N. V, Gillis, R., Fiorese, C. J., and Haynes, C. M. (2014) Mitochondrial UPR-regulated innate immunity provides resistance to pathogen infection. *Nature*. **516**, 414–7
12. Bakowski, M., Desjardins, C., Smelkinson, M., Dunbar, T., Lopez-Moyado, I., Rifkin, S., Cuomo, C., and Troemel, E. (2014) Ubiquitin-Mediated Response to Microsporidia and Virus Infection in C. elegans. *PLoS Pathog.* 10.1371/journal.ppat.1004200
13. Reddy, K. C., Dror, T., Sowa, J. N., Panek, J., Chen, K., Lim, E. S., Wang, D., and Troemel, E. R. (2017) An Intracellular Pathogen Response Pathway Promotes Proteostasis In C. elegans. *Curr. Biol.* 10.1016/j.cub.2017.10.009
14. Zhang, G., Sachse, M., Prevost, M.-C., Luallen, R. J., Troemel, E. R., and Félix, M.-A. (2016) A Large Collection of Novel Nematode-Infecting Microsporidia and Their Diverse Interactions with

Caenorhabditis elegans and Other Related Nematodes. *PLOS Pathog.* **12**, e1006093
15. Sarkies, P., Ashe, A., Le Pen, J., McKie, M. A., and Miska, E. A. (2013) Competition between virus-derived and endogenous small RNAs regulates gene expression in Caenorhabditis elegans. *Genome Res.* **23**, 1258–1270
16. Chen, K., Franz, C. J., Jiang, H., Jiang, Y., and Wang, D. (2017) An evolutionarily conserved transcriptional response to viral infection in Caenorhabditis nematodes. *BMC Genomics*. **18**, 303
17. Reddy, K. C., Dror, T., Underwood, R. S., Osman, G. A., Elder, C. R., Desjardins, C. A., Cuomo, C. A., Barkoulas, M., and Troemel, E. R. (2019) Antagonistic paralogs control a switch between growth and pathogen resistance in C. elegans. *PLOS Pathog.* **15**, e1007528
18. Hsu, A.-L., Murphy, C. T., and Kenyon, C. (2003) Regulation of Aging and Age-Related Disease by DAF-16 and Heat-Shock Factor. *Science*. **300**, 1142–1145
19. Li, X., Matilainen, O., Jin, C., Glover-Cutter, K. M., Holmberg, C. I., and Blackwell, T. K. (2011) Specific SKN-1/NrF stress responses to perturbations in translation elongation and proteasome activity. *PLoS Genet.* **7**, 9–11
20. Lehrbach, N. J., and Ruvkun, G. (2016) Proteasome dysfunction triggers activation of SKN-1A/Nrf1 by the aspartic protease DDI-1. *Elife*. 10.7554/eLife.17721
21. Radhakrishnan, S. K., Lee, C. S., Young, P., Beskow, A., Chan, J. Y., and Deshaies, R. J. (2010) Transcription Factor Nrf1 Mediates the Proteasome Recovery Pathway after Proteasome Inhibition in Mammalian Cells. *Mol. Cell*. **38**, 17–28
22. Zheng, N., and Shabek, N. (2017) Ubiquitin Ligases: Structure, Function, and Regulation. *Annu. Rev. Biochem.* **86**, 129–157
23. Petroski, M. D., and Deshaies, R. J. (2005) Function and regulation of cullin–RING ubiquitin ligases. *Nat. Rev. Mol. Cell Biol.* **6**, 9–20
24. Thomas, J. H. (2006) Adaptive evolution in two large families of ubiquitin-ligase adapters in nematodes and plants. *Genome Res.* **16**, 1017–30
25. Kipreos, E. (2005) Ubiquitin-mediated pathways in C. elegans. *WormBook*. 10.1895/wormbook.1.36.1
26. Jin, J., Cardozo, T., Lovering, R. C., Elledge, S. J., Pagano, M., and Harper, J. W. (2004) Systematic analysis and nomenclature of mammalian F-box proteins. *Genes Dev.* **18**, 2573–2580
27. Kipreos, E. T., and Pagano, M. (2000) The F-box protein family. *Genome Biol.* **1**, REVIEWS3002
28. Nayak, S., Santiago, F. E., Jin, H., Lin, D., Schedl, T., and Kipreos, E. T. (2002) The *Caenorhabditis elegans* Skp1-related gene family: diverse functions in cell proliferation, morphogenesis, and meiosis. *Curr. Biol.* **12**, 277–87
29. Duda, D. M., Borg, L. A., Scott, D. C., Hunt, H. W., Hammel, M., and Schulman, B. A. (2008) Structural Insights into NEDD8 Activation of Cullin-RING Ligases: Conformational Control of Conjugation. *Cell*. **134**, 995–1006
30. Frøkjær-Jensen, C., Davis, M. W., Ailion, M., and Jorgensen, E. M. (2012) Improved Mos1-mediated transgenesis in C. elegans. *Nat. Methods*. **9**, 117–118
31. Sarov, M., Murray, J. I., Schanze, K., Pozniakovski, A., Niu, W., Angermann, K., Hasse, S., Rupprecht, M., Vinis, E., Tinney, M., Preston, E., Zinke, A., Enst, S., Teichgraber, T., Janette, J., Reis, K., Janosch, S., Schloissnig, S., Ejsmont, R. K., Slightam, C., Xu, X., Kim, S. K., Reinke, V., Stewart, A. F., Snyder, M., Waterston, R. H., Hyman, A. A., Radoslaw, K., Slightam, C., Xu, X., Kim, S. K., Reinke, V., Stewart, A. F., Snyder, M., Waterston, R. H., and Hyman, A. A. (2012) A genome scale resource for in vivo tag-based protein function exploration in C. elegans. *Cell*. **150**, 855–866
32. Wu, K., Chen, A., and Pan, Z.-Q. (2000) Conjugation of Nedd8 to CUL1 Enhances the Ability of the ROC1-CUL1 Complex to Promote Ubiquitin Polymerization. *J. Biol. Chem.* **275**, 32317–32324
33. Hatakeyama, S. (2017) TRIM Family Proteins: Roles in Autophagy, Immunity, and Carcinogenesis. *Trends Biochem. Sci.* **42**, 297–311
34. Sardiello, M., Cairo, S., Fontanella, B., Ballabio, A., and Meroni, G. (2008) Genomic analysis of

the TRIM family reveals two groups of genes with distinct evolutionary properties. *BMC Evol. Biol.* **8**, 225

35. Pang, S., and Curran, S. P. (2014) Adaptive Capacity to Bacterial Diet Modulates Aging in C. elegans. *Cell Metab.* **19**, 221–231
36. Lynn, D. A., Dalton, H. M., Sowa, J. N., Wang, M. C., Soukas, A. A., and Curran, S. P. (2015) Omega-3 and -6 fatty acids allocate somatic and germline lipids to ensure fitness during nutrient and oxidative stress in *Caenorhabditis elegans*. *Proc. Natl. Acad. Sci.* **112**, 15378–15383
37. Leyva-Díaz, E., Stefanakis, N., Carrera, I., Glenwinkel, L., Wang, G., Driscoll, M., and Hobert, O. (2017) Silencing of Repetitive DNA Is Controlled by a Member of an Unusual *Caenorhabditis elegans* Gene Family. *Genetics*. **207**, genetics.300134.2017
38. Dawidziak, D. M., Sanchez, J. G., Wagner, J. M., Ganser-Pornillos, B. K., and Pornillos, O. (2017) Structure and catalytic activation of the TRIM23 RING E3 ubiquitin ligase. *Proteins*. **85**, 1957–1961
39. Mongkoldhumrongkul, N., Swain, S. C., Jayasinghe, S. N., and Stürzenbaum, S. (2010) Bio-electrospraying the nematode *Caenorhabditis elegans* : studying whole-genome transcriptional responses and key life cycle parameters. *J. R. Soc. Interface*. **7**, 595–601
40. Tawo, R., Pokrzywa, W., Kevei, É., Akyuz, M. E., Balaji, V., Adrian, S., Höhfeld, J., and Hoppe, T. (2017) The Ubiquitin Ligase CHIP Integrates Proteostasis and Aging by Regulation of Insulin Receptor Turnover. *Cell*. **169**, 470–482.e13
41. Koren, I., Timms, R. T., Kula, T., Xu, Q., Li, M. Z., and Elledge, S. J. (2018) The Eukaryotic Proteome Is Shaped by E3 Ubiquitin Ligases Targeting C-Terminal Degrons. *Cell*. **173**, 1622–1635.e14
42. Lin, H.-C., Yeh, C.-W., Chen, Y.-F., Lee, T.-T., Hsieh, P.-Y., Rusnac, D. V., Lin, S.-Y., Elledge, S. J., Zheng, N., and Yen, H.-C. S. (2018) C-Terminal End-Directed Protein Elimination by CRL2 Ubiquitin Ligases. *Mol. Cell*. **70**, 602–613.e3
43. Gibson, D. G., Young, L., Chuang, R.-Y., Craig Venter, J., Hutchison III, C. A., Smith, H. O., Venter, J. C., Hutchison, C. A., and Smith, H. O. (2009) Enzymatic assembly of DNA molecules up to several hundred kilobases. *Nat. Methods*. **6**, 343–345
44. Gendron, J. M., Webb, K., Yang, B., Rising, L., Zuzow, N., and Bennett, E. J. (2016) Using the Ubiquitin-modified Proteome to Monitor Distinct and Spatially Restricted Protein Homeostasis Dysfunction. *Mol. Cell. Proteomics*. **15**, 2576–93
45. Zhang, X., Smits, A. H., van Tilburg, G. B., Ovaa, H., Huber, W., and Vermeulen, M. (2018) Proteome-wide identification of ubiquitin interactions using UbIA-MS. *Nat. Protoc.* **13**, 530–550
46. Capella-Gutierrez, S., Silla-Martinez, J. M., and Gabaldon, T. (2009) trimAl: a tool for automated alignment trimming in large-scale phylogenetic analyses. *Bioinformatics*. **25**, 1972–1973
47. Sanchez, R., Serra, F., Tarraga, J., Medina, I., Carbonell, J., Pulido, L., de Maria, A., Capella-Gutierrez, S., Huerta-Cepas, J., Gabaldon, T., Dopazo, J., and Dopazo, H. (2011) Phylemon 2.0: a suite of web-tools for molecular evolution, phylogenetics, phylogenomics and hypotheses testing. *Nucleic Acids Res.* **39**, W470–W474
48. Suchard, M. A., Lemey, P., Baele, G., Ayres, D. L., Drummond, A. J., and Rambaut, A. (2018) Bayesian phylogenetic and phylodynamic data integration using BEAST 1.10. *Virus Evol.* **4**, vey016

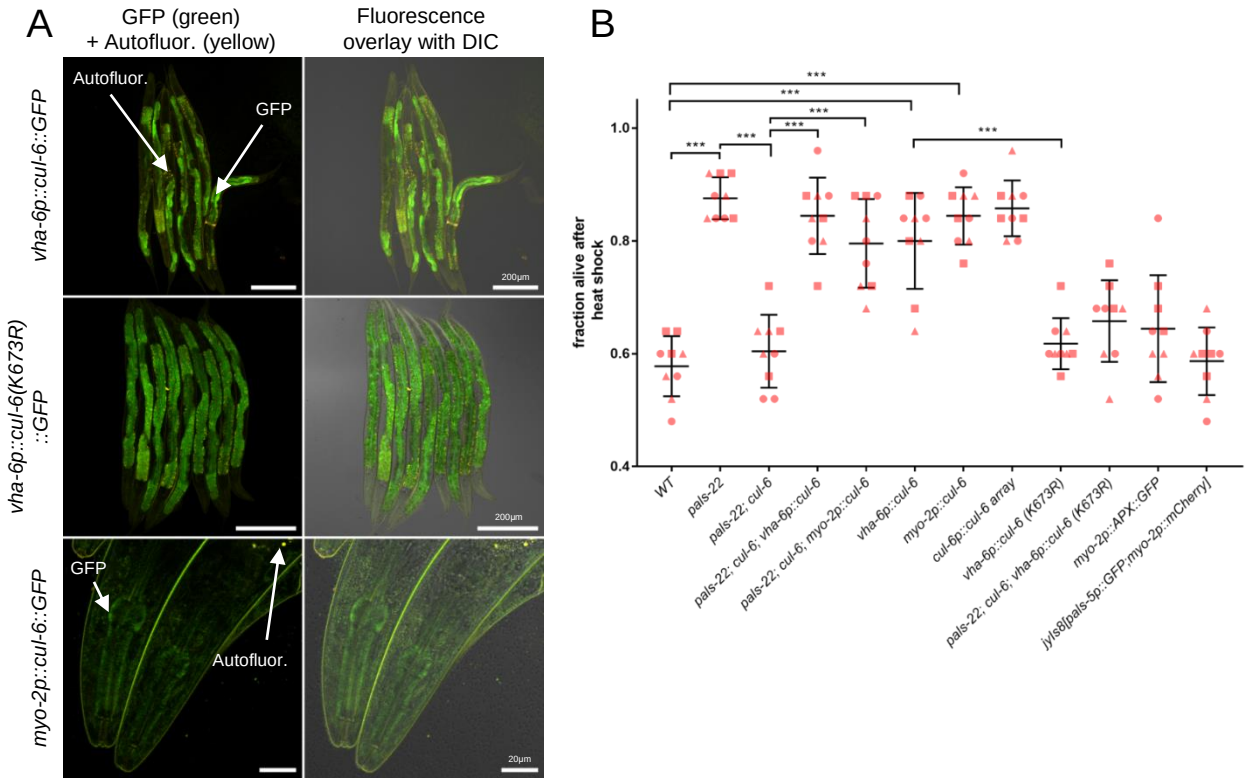

Figure 1. CUL-6 expression in the intestine or in the pharynx promotes thermotolerance
(A) Confocal fluorescence images of adult animals with *cul-6::GFP* transgenes driven by *vha-6* or *myo-2* promoter and integrated with MosSCI. Autofluorescence is indicated by the overlay of the red and green channels. (B) Survival of animals after 2 h 37.5°C heat shock treatment, followed by 24 h at 20°C. Strains were tested in triplicate experiments, with three plates per experiment, 30 animals per plate. The genotypes *myo-2p::APX::GFP* and *jyIs8[pals-5p::GFP;myo-2p::mCherry]* were tested as controls for *myo-2p* driven expression. Each dot represents a plate, and different shapes represent the experimental replicates done on different days. Mean fraction alive of the nine replicates is indicated by black bar with errors bars as SD. *** $p < 0.001$, ** $p < 0.01$, * $p < 0.05$, n.s. $p > 0.05$ with one-way ANOVA and Tukey's HSD for post-hoc multiple comparisons.

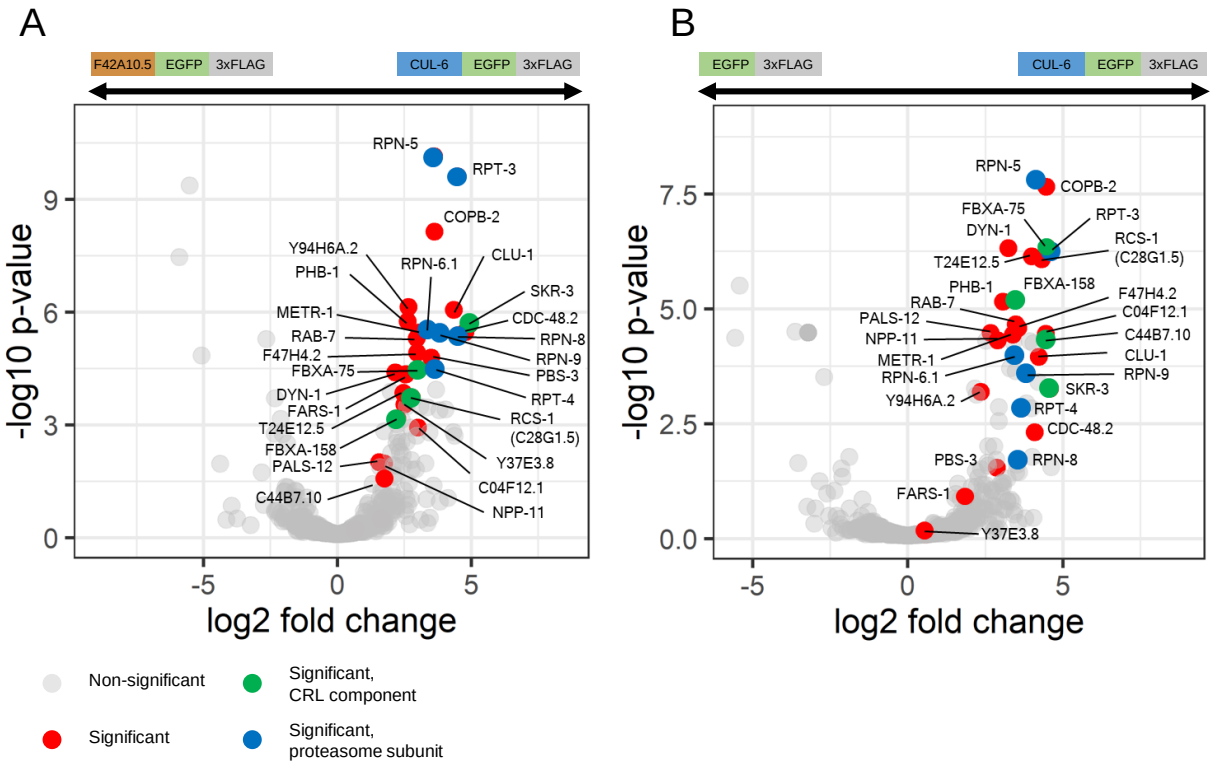

Figure 2. Co-immunoprecipitation mass spectrometry analysis identifies binding partners for CUL-6

Volcano plot of proteins significantly enriched in CUL-6 IP compared to F42A10.5 (A) or to GFP IP (B). Proteins significantly more abundant compared to either of the control IPs (GFP alone control or F42A10.5 control, at adjusted p-value < 0.05 and log2 fold change > 1) were considered interacting proteins (Supplementary Table 1). Baits were removed from the graphs. Gray dots indicate non-significant proteins, red dots indicate significant proteins, green dots indicate significant CRL proteins and blue dots indicate significant proteasome subunits.

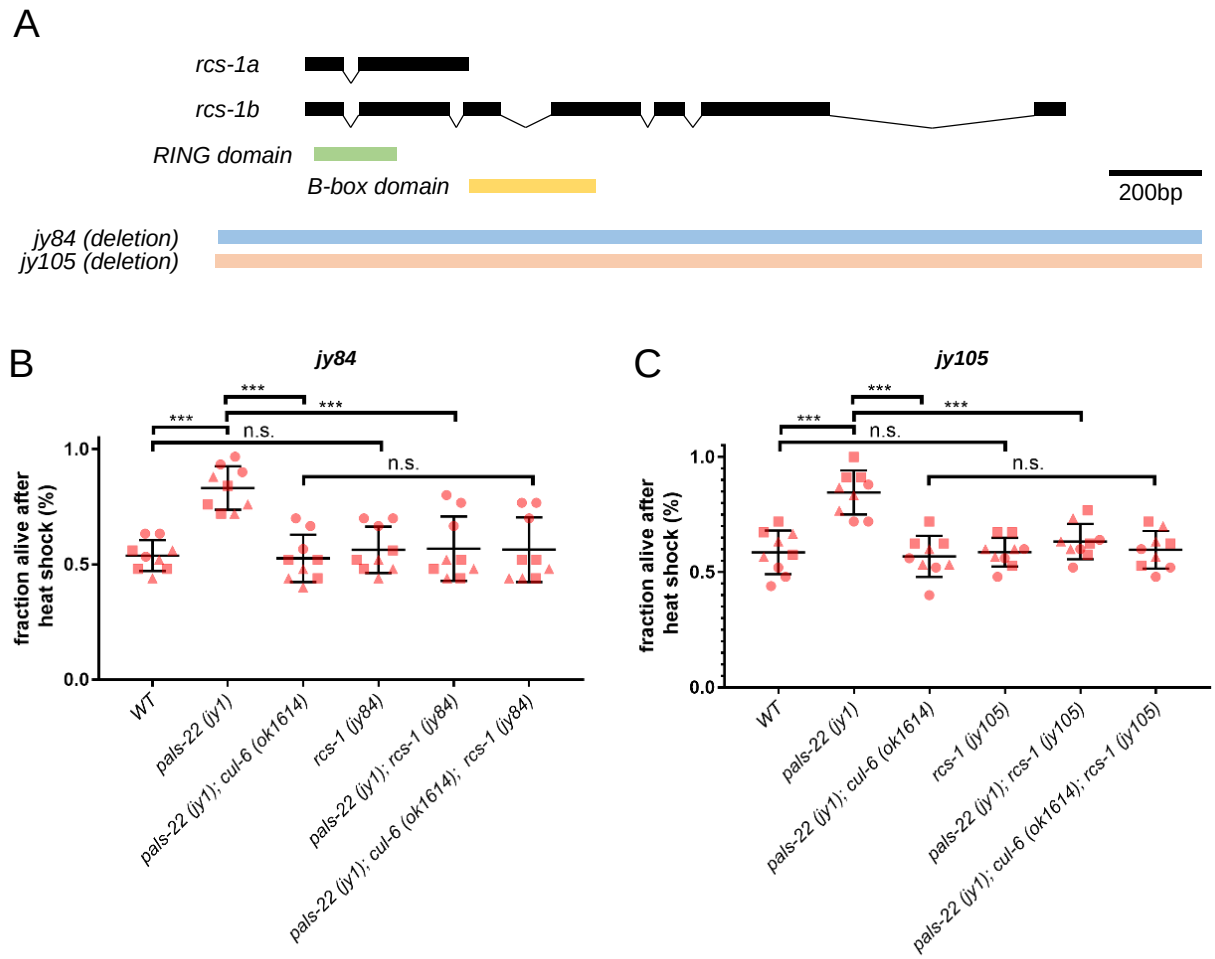

Figure 3. RING domain protein RCS-1 (C28G1.5) promotes thermotolerance in *pals-22* mutants. (A) *rcs-1* isoforms and exon/intron structure. Protein domains colored in green and yellow. *jy84* and *jy105* are deletion alleles. (B and C) Survival of animals after 2 h 37.5°C heat shock treatment, followed by 24 h at 20°C. Strains were tested in triplicate experiments, with three plates per experiment, 30 animals per plate. Each dot represents a plate, and different shapes represent the experimental replicates done on three different days. Mean fraction alive of the nine replicates is indicated by black bar with errors bars as SD. *** $p < 0.001$, ** $p < 0.01$, * $p < 0.05$, n.s. $p > 0.05$ one-way ANOVA and Tukey's HSD for post-hoc multiple comparisons.

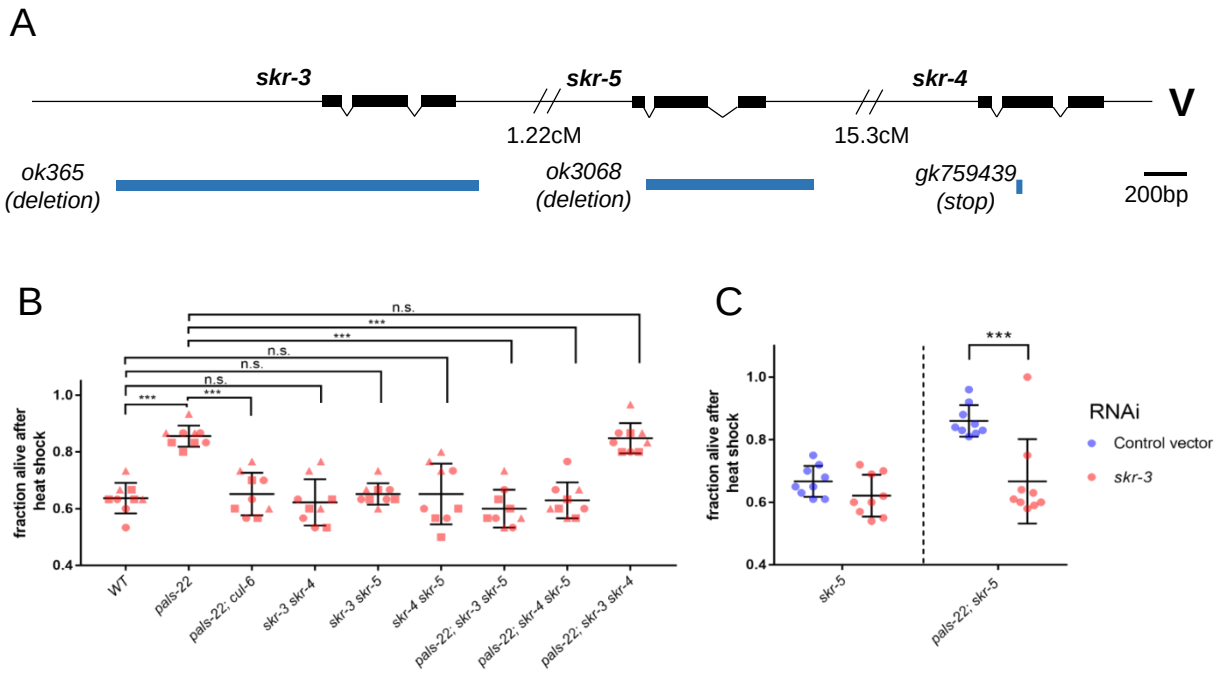

Figure 4. SKR-3, SKR-4 and SKR-5 act redundantly to promote thermotolerance in *pals-22* mutants

(A) *skr-3*, *skr-4* and *skr-5* gene exon/intron structure. *ok365* and *ok3068* are deletion alleles, *gk759439* is a premature stop mutation. (B) Survival of animals after 2 h 37.5°C heat shock treatment, followed by 24 h at 20°C. Strains were tested in triplicate experiments, with three plates per experiment, 30 animals per plate. Each dot represents a plate, and different shapes represent the experimental replicates done on different days. (C) Survival of animals after 2 h 37.5°C heat shock treatment, followed by 24 h at 20°C. *skr-5* and *skr-5*; *pals-22* mutants were fed on (R)OP50 expressing either L4440 (empty vector) *cul-6* or *skr-3* RNAi. Each dot represents a plate, mean fraction alive of the nine replicates is indicated by black bar with errors bars as SD. *** $p < 0.001$, ** $p < 0.001$, n.s. $p > 0.05$ with one way ANOVA and Tukey's HSD for post-hoc multiple comparisons.

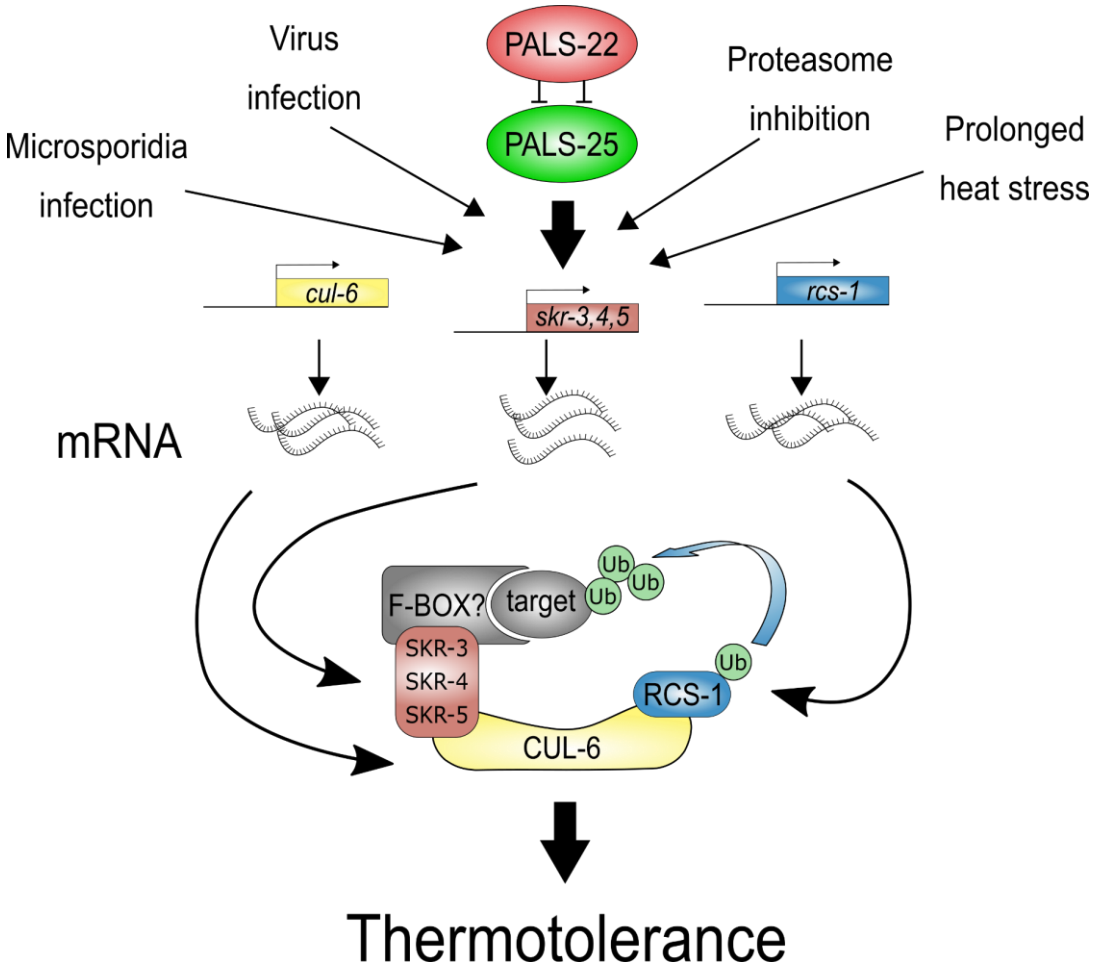

Figure 5 Model for a RCS-1/CUL-6/SKR ubiquitin ligase that promotes proteostasis

A

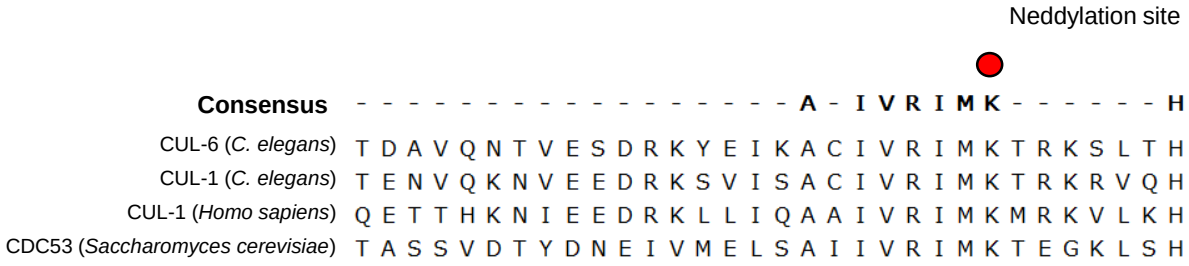

Supplementary Figure 1. Alignment of C-terminal region of *cul-6* with other cullin genes.
Conserved lysine residue targeted by neddylation is indicated by a red circle.

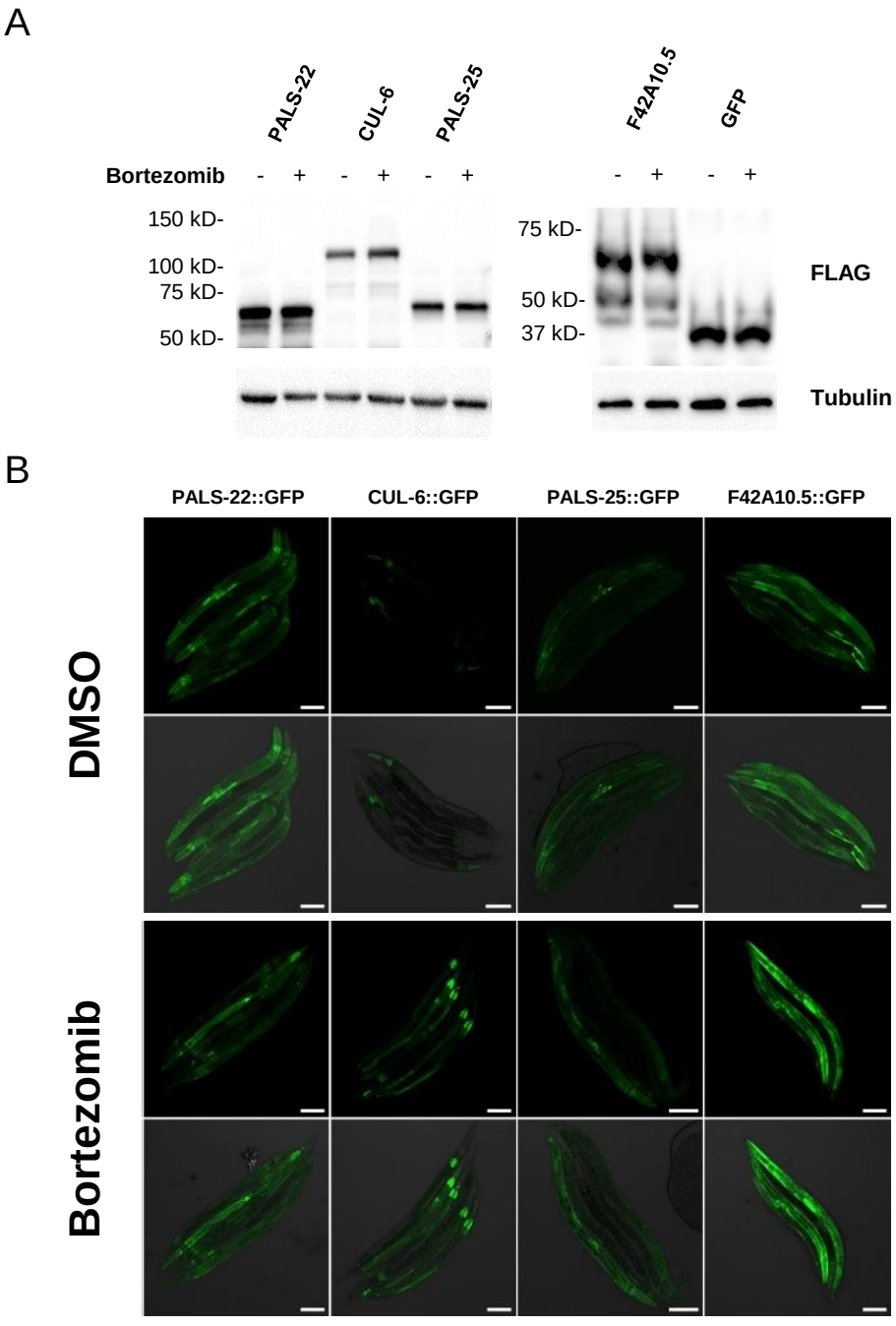

Supplementary Figure 2. Expression analysis of GFP::3xFLAG-tagged proteins used for Co-IP/MS studies

(A) Western blot analysis of total protein lysate from transgenic adult animals containing fosmid transgenes expressing GFP::3xFLAG tagged protein and treated with Bortezomib or DMSO as diluent control. Proteins were detected with anti-FLAG, and anti-tubulin antibody was used as a loading control. Expected sizes: CUL-6::GFP::3xFLAG (116 kD), PALS-22::GFP::3xFLAG (64.8 kD), PALS-25 GFP::3xFLAG (66.9 kD), F42A10.5 GFP::3xFLAG (61.3 kD), GFP-3::FLAG (34 kD). (B) Confocal fluorescence images of L4 animals with fosmid transgenes expressing GFP-tagged proteins from endogenous promoters, after exposure to DMSO or Bortezomib (diluted in DMSO). Images are overlays of green and phase contrast channels. Scale bar is 100 µm.

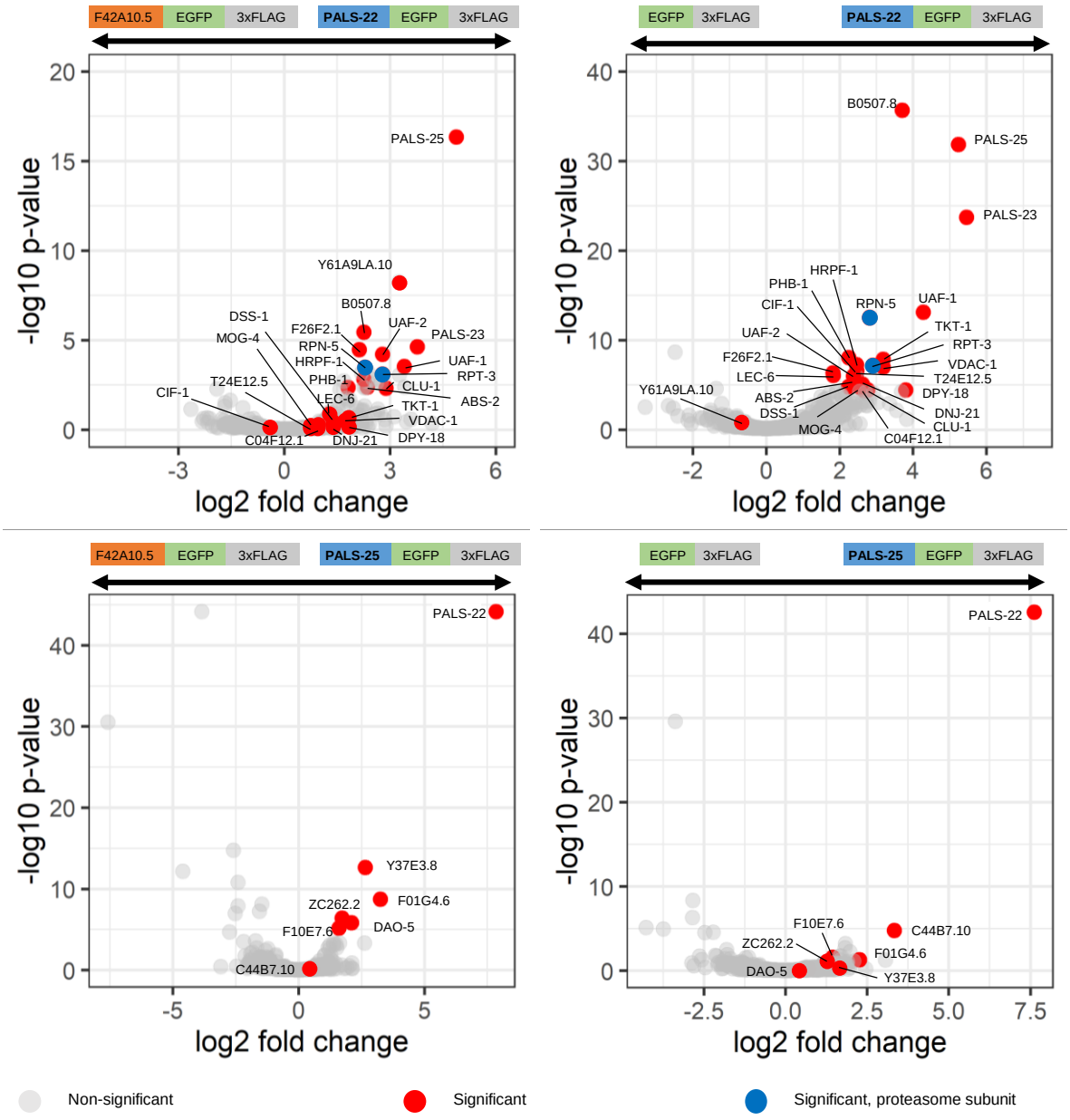

Supplementary Figure 3 Co-immunoprecipitation mass spectrometry analysis identifies binding partners for PALS-22 and PALS-25

Volcano plot of proteins significantly enriched in PALS-22 and PALS-25 IPs compared to F42A10.5 IP or GFP IP. Proteins significantly more abundant compared to either of the control IP's (GFP alone control or F42A10.5 control, at adjusted p-value < 0.05 and log2 fold change > 1) were considered interacting proteins (Supplementary Table 1). Baits were removed from the graphs. Gray dots indicate non-significant proteins, red dots indicate significant proteins and blue dots indicate significant proteasome subunits.

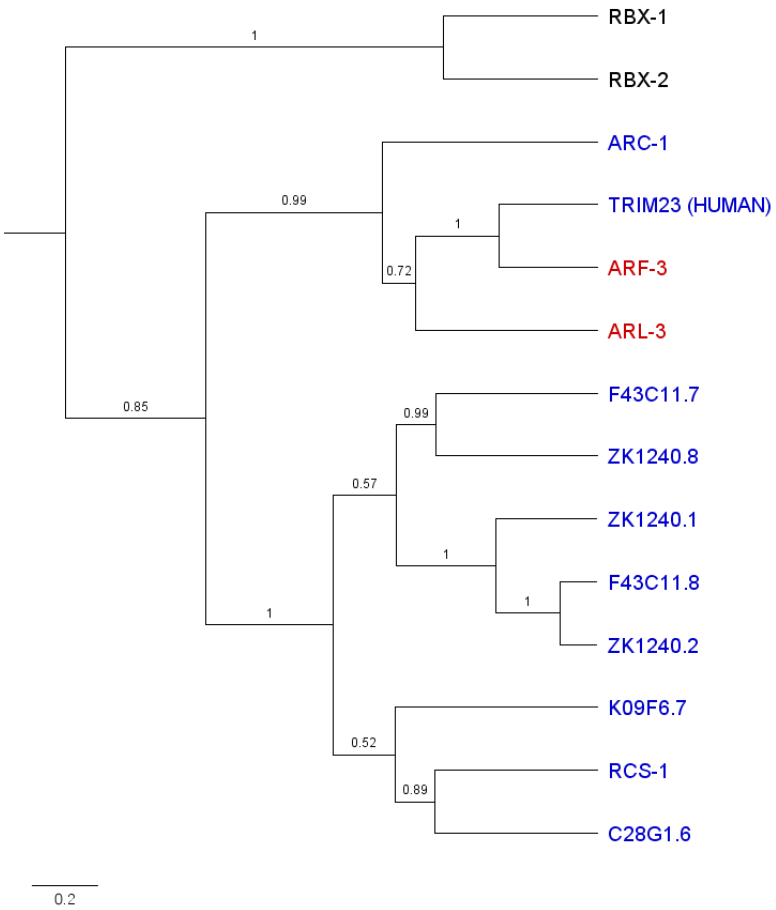

Supplementary Figure 4. Phylogenetic tree of RCS-1

Phylogenetic relationships of RCS-1 protein with TRIM23 homologs proteins (in red), canonical RBX proteins (in black) and known TRIM *C. elegans* proteins (in blue). All proteins are from *C. elegans*, except TRIM23. The tree was built from a protein alignment using the Bayesian MCMC method. Posterior probabilities are indicated on the branches.

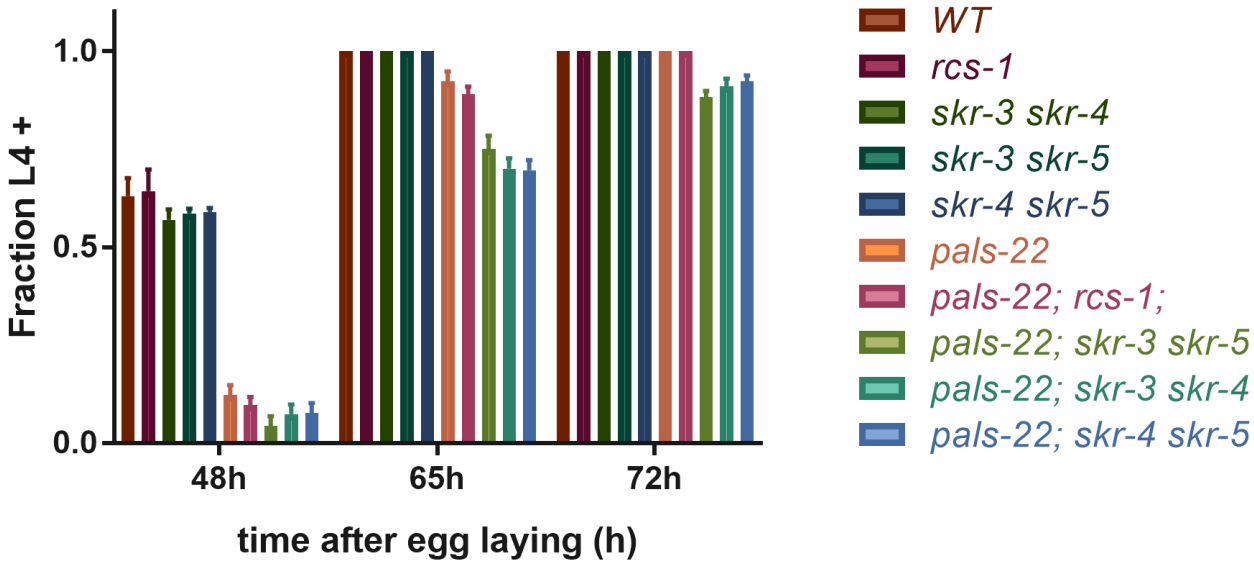

Supplementary Figure 5 Analysis of developmental timing for *pals-22, rcs-1* and *skr* mutants
skr double and triple mutants in a *pals-22* background do not suppress the developmental delay of *pals-22* mutants. Percentage of animals reaching the L4 larval stage at time points after eggs were laid is indicated. Results shown are the average of 3 independent biological replicates, with 100 animals assayed in each replicate.

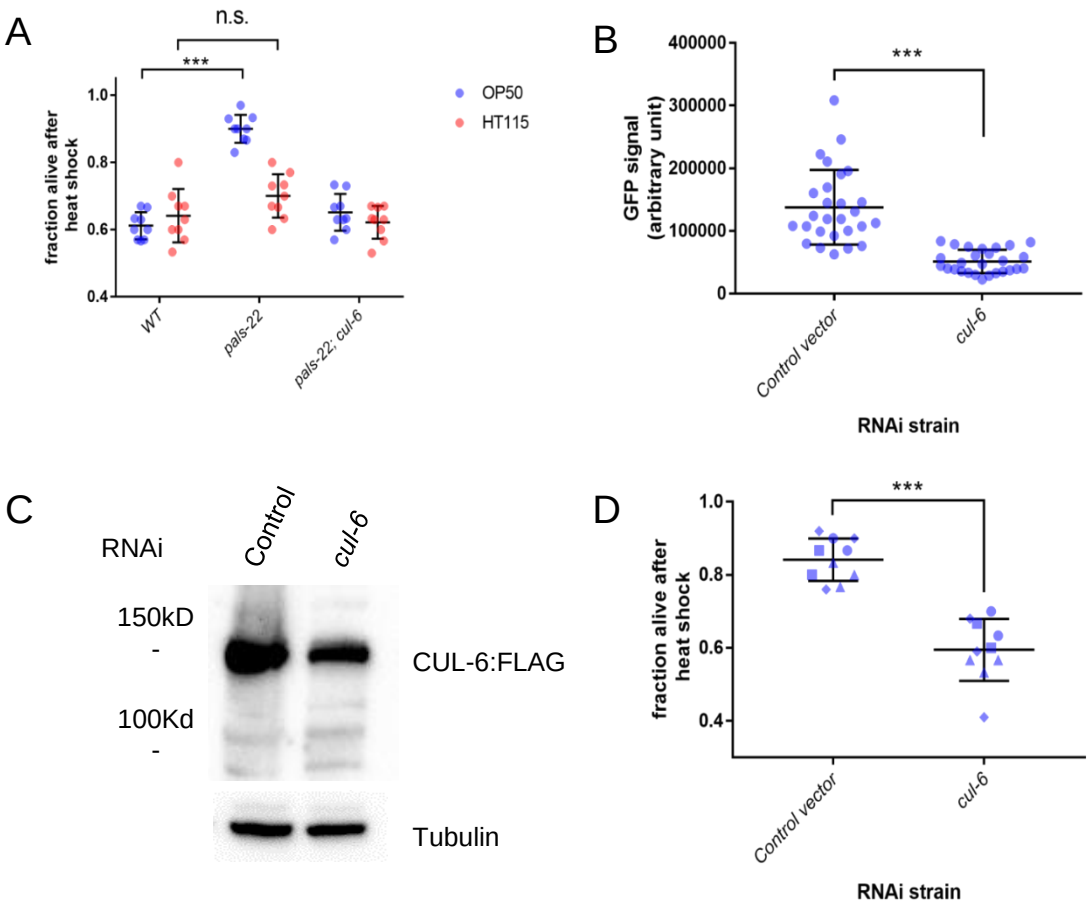

Supplementary Figure 6. Development of an RNAi system for analyzing thermotolerance in *pals-22* mutants

(A) Survival of animals after 2 h 37.5°C heat shock treatment, followed by 24 h at 20°C either fed on OP50 strain (R)OP50 or HT115 *E. coli*. Each dot represents a plate. Mean fraction alive of the ten replicates is indicated by black bar with errors bars as SD. *** $p < 0.001$ with Student's t-test. (B) Quantification of GFP signal in L4 animal expressing CUL-6::GFP grown on (R)OP50 expressing either L4440 (control vector) or *cul-6* RNAi. GFP Signal was measured with ImageJ in the pharynx and the first intestinal cells ring together with 3 adjacent background regions and the Total Corrected Fluorescence (TCF) was calculated. Error bars are SD. *** $p < 0.001$ with Student's t-test. (C) Western blot analysis on total protein lysate from adult animals with fosmid transgenes expressing CUL-6::GFP::3XFLAG treated with control or *cul-6* RNAi (OP50). CUL-6::GFP::3XFLAG protein was detected with anti-FLAG, and anti-tubulin antibody was used as a loading control. (D) Survival of *pals-22* mutants after 2 h 37.5°C heat shock treatment, followed by 24 h at 20°C. animals fed on (R)OP50 expressing either L4440 (control vector) or *cul-6* RNAi. Each dot represents a plate, and different shapes represent the experimental replicates done on different days. Mean fraction alive of the nine replicates is indicated by black bar with errors bars as SD. *** $p < 0.001$ with Student's t-test.

Supplementary Table 1. Statistical analysis of co-IP experiments.
Each tab shows the fold change and adjusted p-values between one experimental IPs and the two control IP's. Each tab shows results for one experimental IP.

Supplementary Table 2. List of the C. elegans strains and DNA constructs used in this publication.